Density functional theory study of the structural, electronic, lattice dynamical, and thermodynamic properties of Li_4SiO_4 and its capability for CO_2 capture

Yuhua Duan[1,*] and K. Parlinski[2]

[1]*National Energy Technology Laboratory, United States Department of Energy, Pittsburgh, Pennsylvania 15236, USA*

[2]*Institute of Nuclear Physics, Polish Academy of Sciences, Radzikowskiego 152, 31-341 Kraków, Poland*

(Received 31 May 2011; published 9 September 2011)

The structural, electronic, lattice dynamical, optical, thermodynamic, and CO_2 capture properties of monoclinic and triclinic phases of Li_4SiO_4 are investigated by combining density functional theory with phonon lattice dynamics calculations. We found that these two phases have some similarities in their bulk and thermodynamic properties. The calculated bulk modulus and the cohesive energies of these two phases are close to each other. Although both of them are insulators, the monoclinic phase of Li_4SiO_4 has a direct band gap of 5.24 eV while the triclinic Li_4SiO_4 phase has an indirect band gap of 4.98 eV. In both phases of Li_4SiO_4, the *s* orbital of O mainly contributes to the lower-energy second valence band (VB_2) and the *p* orbitals contribute to the fist valence band (VB_1) and the conduction bands (CBs). The *s* orbital of Si mainly contributes to the lower portions of the VB_1 and VB_2, and Si *p* orbitals mainly contribute to the higher portions of the VB_1 and VB_2. The *s* and *p* orbitals of Li contribute to both VBs and to CBs, and Li *p* orbitals have a higher contribution than the Li *s* orbital. There is possibly a phonon soft mode existing in triclinic γ-Li_4SiO_4; in the monoclinic Li_4SiO_4, there are three phonon soft modes, which correspond to the one type of Li disordered over a few sites. Their LO-TO splitting indicates that both phases of Li_4SiO_4 are polar anisotropic materials. The calculated infrared absorption spectra for LO and TO modes are different for these two phases of Li_4SiO_4. The calculated relationships of the chemical potential versus temperature and CO_2 pressure for reaction of Li_4SiO_4 with CO_2 shows that Li_4SiO_4 could be a good candidate for a high-temperature CO_2 sorbent while used for postcombustion capture technology.

DOI: 10.1103/PhysRevB.84.104113 PACS number(s): 63.20.dk, 64.10.+h, 78.20.−e

I. INTRODUCTION

As solid electrolytes, lithium silicates (e.g., Li_4SiO_4 and Li_2SiO_3) are widely used in high-energy lithium secondary batteries due to their better energies per unit weight, high melting point, and high lithium ion conductivity.[1,2] Due to their low chemical reactivity with water and excellent compatibility with other materials, lithium ceramics are the best option for tritium production and release through the $^6Li + n_t \rightarrow {}^3T + {}^4He$ reaction, which determines the possible application of a tritium breeder material into the fusion reactors.[3–8]

In recent decades, another possible application for lithium silicates has been found: as CO_2 sorbents to fight global warming.[9–11] Nakagawa and Ohashi[9,10] reported a novel method to capture CO_2 from high-temperature gases though the reversible reaction $Li_4SiO_4 + CO_2 \leftrightarrow Li_2SiO_3 + Li_2CO_3$, where Li_4SiO_4 as CO_2 absorbent maintains its absorption effectiveness during the cycle between absorption at 973 K and emission at 1123 K in the case of following pure CO_2 at a total pressure of 1.0×10^5 Pa.[12–14]

In the literature, there are only few theoretical studies on the electronic structure of crystalline lithium silicates. Based on the linear combination of atomic orbitals and Hartree-Fock (LCAO-HF) *ab initio* calculations, Munakata and Yokoyama[15] calculated the electronic state of Li_4SiO_4 and obtained a wide band gap of 17.5 eV. With an *ab initio* approach, Uchino and Yoko[16,17] investigated the local coordination environments of alkali cations (Li^+ and Na^+) in a cluster model of single- and mixed-alkali silicate glasses. Their results demonstrated that the average coordination number of alkali cations increased from Li to Na, and each alkali cation is located in rather individual local sites in both single- and mixed-alkali clusters. Employing the orthogonalized linear combination of atomic orbitals method, Ching *et al.*[18] calculated the electronic structures of Li_2SiO_3 and $Li_2Si_2O_5$ and compared them with x-ray photoelectron spectroscopy measurements. Their results showed that the effective charge on Li is quite small (0.07e in Li_2SiO_3 and 0.02e in $Li_2Si_2O_5$). Du and Corrales[19,20] employed density functional theory (DFT) to characterize the structural and electronic properties of alkali silicate glasses [$xM_2O - (100 - x)SiO_2$, where M = Li, Na, K], Li_2SiO_3, and $Li_2Si_2O_5$. Their results revealed clear differences between the bridging and the nonbridging oxygen ions through all valence bands (VBs). With *ab initio* molecular orbital calculations, Nakazawa *et al.*[21] investigated the chemical nature of superficial hydrogen on the lithium silicate doped with B, Al, and Ga. Their results showed that the iconicity of surface hydrogen is strengthened by the interaction of the electron acceptor (dopant units) with surface oxygen but weakened by a Li atom bonded to nonbridging oxygen. Cruz *et al.*[6] analyzed the kinetics of the thermal decomposition of Li_4SiO_4 and Li_2SiO_3 and found that Li_4SiO_4 began to decompose between 900 °C and 1000 °C and to melt above 1100 °C, whereas Li_2SiO_3 is highly stable at the temperatures studied. Assuming a mechanism of diffusion-controlled reaction into a spherical system, they estimated that the activation energy for this process is 331 kJ/mol. To our knowledge, no comprehensive theoretical study on Li_4SiO_4 (specifically, the triclinic phase) has been done to investigate the electronic and thermodynamic properties.

In this study, applying first-principles DFT, the electronic and the lattice dynamical properties of monoclinic and triclinic phases of Li_4SiO_4 were thoroughly investigated. Based on the calculated energetic and thermodynamic properties of the solids, the capacities of Li_4SiO_4 as a sorbent to capture CO_2 were evaluated.

This paper is organized as follows: in the second section we briefly describe the theoretical method, in the third section we show our results for Li_4SiO_4 crystals and compare these with other available reports, and in the last section we summarize our conclusions.

II. THEORETICAL METHODS

The calculations performed in this work were based on first-principles DFT with plane-wave basis sets and the pseudopotential to describe the electron–ion interactions. The Vienna *ab initio* simulation package[22,23] was employed to calculate the electronic structures of the lithium silicate and lithium carbonate materials. From our previous experience on oxides and salts,[24–28] we employed projector augmented wave pseudopotential and PW91 exchange-correlation functions.[29] Plane-wave basis sets were used with a kinetic energy cutoff of 520 eV and an augmentation charge cutoff of 605.4 eV. The k-point sampling grids of $m \times n \times l$, obtained using the Monkhorst-Pack method,[30] were used for these bulk calculations, where m, n, and l are determined by the spacing of ~ 0.028 Å^{-1} along the reciprocal a, b, and c axes of their unit cells, respectively.

The corresponding k-points sets were $3 \times 6 \times 2$ and $8 \times 9 \times 9$ for monoclinic Li_4SiO_4 and triclinic γ-Li_4SiO_4, respectively. The valence electrons contain s and p orbitals for Li, O, and Si atoms. During calculations, we relaxed all atoms in the cell to their optimized structure. For the band structure calculations, the symbols and coordinates of the high-symmetry points in the crystals were taken from Bradley and Cracknell's definitions.[31] Based on the density functional perturbation theory (DFPT),[32–34] the Born effective charges were calculated and used in phonon calculations to obtain the infrared (IR) absorption.

In this study, we employed the Phonon software package,[35] in which the direct method is applied, to be combined *ab initio* DFPT. Similar to our previous approach,[24,25,27] the phonon dispersion and the thermodynamic properties (free energy change, entropy change, etc.) can be carried out for each crystal. In turn, the zero-point energy change and the phonon free energy change are obtained and used for analyzing the thermodynamic stabilities. The long-range electric fields associated with long-wave longitudinal phonons are responsible for the longitudinal optical (LO)–transverse optical (TO) splitting that removes the degeneracy between LO and TO phonons at the Brillion zone center.[36] With the Born effective charges obtained from DFPT, the LO-TO splitting and the IR spectrum can be obtained.

In phonon calculations, a $1 \times 2 \times 1$ supercell for monoclinic Li_4SiO_4 and $2 \times 3 \times 3$ supercell for triclinic γ-Li_4SiO_4 were created from their optimized unit cells that were calculated through DFT. With a displacement of ± 0.03 Å of nonequivalent atoms, a set of displaced supercells was generated. For monoclinic Li_4SiO_4, the set contains 282 different displaced supercells; for triclinic γ-Li_4SiO_4, the number of displaced supercells is 54. For each displaced supercell, the DFPT/DFT calculations were performed again to obtain the Born effective charge and the force on each atom due to the displacements. These forces were carried back to the Phonon package[35] to calculate the phonon dispersion curves and density of states. The partition functions of solid systems can be found from the calculated phonon dispersions and densities of states. With the calculated partition functions, their thermodynamic properties, such as internal energy, free energy, entropy, heat capacity, etc., could be evaluated at different temperatures.[24,25,37]

III. RESULTS AND DISCUSSIONS

A. Crystalline structures and optimizations

The crystal structures of two phases of Li_4SiO_4 are shown in Figure 1, and their experimental crystal structural constants are summarized in Table I. As shown in Fig. 1, lithium orthosilicate (Li_4SiO_4) usually is in a monoclinic structure with space group $P2_1/m$ (No. 11),[38–40] but it has another form (γ-Li_4SiO_4) that is in a triclinic structure with space group $P\bar{1}$ (No. 2).[41] The monoclinic structure of Li_4SiO_4 has 14 units of Li_4SiO_4, which contains seven crystallographically independent groups.[38,40] By averaging the positions of these seven independent groups, a reduced unit cell with 2 units of Li_4SiO_4 is obtained; its structure was reported by Vollenkl *et al.*[39] In the monoclinic superstructure of Li_4SiO_4, the 56 Li atoms are located in 18 individual sites of the subcell out of the 126 possible individual atomic sites. The differences between the structures measured by Dejong *et al.*[38] and by Tranqui *et al.*[40] are that some Li atoms are located in the different sites. In the structure reported by Tranqui *et al.*,[40] all Li atoms have fixed positions with full occupancy, whereas in the structure reported by Dejong *et al.*,[38] four types of Li are half occupied and could form two sets in which the average position of each set is similar in position to the structure reported by Tranqui *et al.*,[40] as shown by the large (green) balls in Fig. 1(a). In this study, to simplify the calculations, we use the crystal structure measured by Tranqui *et al.*[40] with fully occupied Li as our initial structure. The γ-Li_4SiO_4 is made at a low temperature and is isotypic with $Na_4[SnO_4]$.[41] The lithium silicates can be synthesized at a high temperature with different mixture ratio of Li_2O and SiO_2. Unlike other lithium silicates, such as Li_2SiO_3, $Li_2Si_2O_5$, $Li_2Si_3O_7$, $Li_6Si_2O_7$, Li_8SiO_6, and SiO_2, in Li_4SiO_4 the tetrahedral [SiO_4] are not directly connected but are instead surrounded by Li atoms, as shown in Fig. 1.

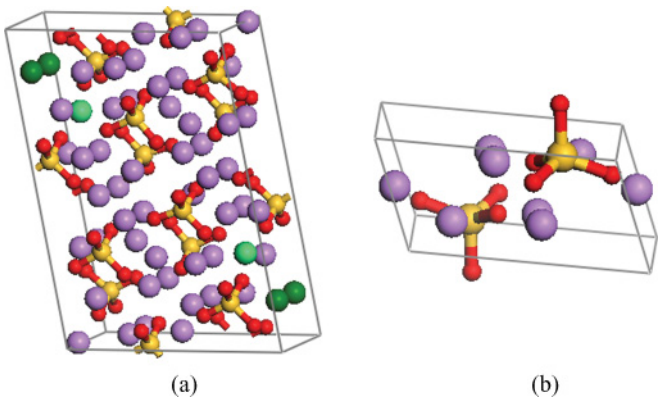

FIG. 1. (Color online) The crystal structures of Li_4SiO_4. Large (purple and green) balls stand for Li, small (red) balls stand for O, the midsize (yellow) ball stands for Si. The c axis is vertical. (a) Monoclinic Li_4SiO_4. (b) Triclinic γ-Li_4SiO_4.

TABLE I. The optimized crystal structural constants in angstroms, fitted parameters of the Birch-Murnaghan equation of state, bulk modulus, and cohesive energy (E_C).

Crystal	Equilibrium structure and deviations (%) Experimental	Optimized	E_0(eV/ unit cell)	B_0 (eV/Å^3)	B_0'	Cell volume V_0(Å^3)	Bulk modulus (GPa)	E_C (eV/f.u.)
Li_4SiO_4	$a=11.532$	$a=11.644(0.97\%)$						
$P2_1/m$(No. 11)[a]	$b=6.075$	$b=6.142(1.10\%)$				1197.3703		
$Z=14$	$c=16.678$	$c=16.875(1.18\%)$	−765.31918	0.46148	4.32844	1153.9(exp)[a]	73.94	54.23
	$\beta=99.04^\circ$	$\beta=99.10^\circ$ (0.05%)						
γ-Li_4SiO_4	$a=7.519$	$a=7.579(0.80\%)$						
$P\bar{1}$ (No. 2)[b]	$b=5.648$	$b=5.678(0.53\%)$						
$Z=2$	$c=5.031$	$c=5.058(0.55\%)$						
	$\alpha=124.15^\circ$	$\alpha=124.21^\circ(0.05\%)$	−109.36221	0.46222	4.56199	171.1617	74.06	54.25
	$\beta=97.18^\circ$	$\beta=97.26^\circ$ (0.08%)				167.21(exp)[b]		
	$\gamma=100.26^\circ$	$\gamma=100.25^\circ(-0.01\%)$						

[a]Ref. 40.
[b]Ref. 41.

To explore their other bulk properties, we calculate their total energies versus the changes of cell volume, as shown in Fig. 2. From it, we can obtain the relationship between energy and volume or pressure by fitting the Birch-Murnaghan equation of state (E-V):[42,43]

$$E(V) = E_0 + \frac{9\times B_0 V_0}{16}\left\{\left[\left(\frac{V_0}{V}\right)^{\frac{2}{3}}-1\right]^3\times B_0' + \left[\left(\frac{V_0}{V}\right)^{\frac{2}{3}}-1\right]^2\times\left[6-4\times\left(\frac{V_0}{V}\right)^{\frac{2}{3}}\right]\right\}. \quad (1)$$

By fitting the data of Fig. 2 to Eq. (1), we obtained the parameters in Eq. (1) for these two phases of Li_4SiO_4, which are listed in Table I. The bulk modulus B is defined as $B = B_0 + B'_0 \times P$ in this scheme, where P is the pressure and here is set to 1 atm. The cohesive energy (E_C) is calculated by subtracting the total bulk energy (E_0 in Table I) from the sum of total energies of the related atoms (e.g., Li, Si, and O) using the same level spin-polarized calculations (in this case, we get $E_{Li} = -0.04403$ eV, $E_{Si} = -0.12847$ eV, and $E_O = -0.12996$ eV) and then dividing by the number of formulas in the unit cell (Z) given in Table I. Our calculated E_C, as well as other values from the literature, are also listed in Table I.

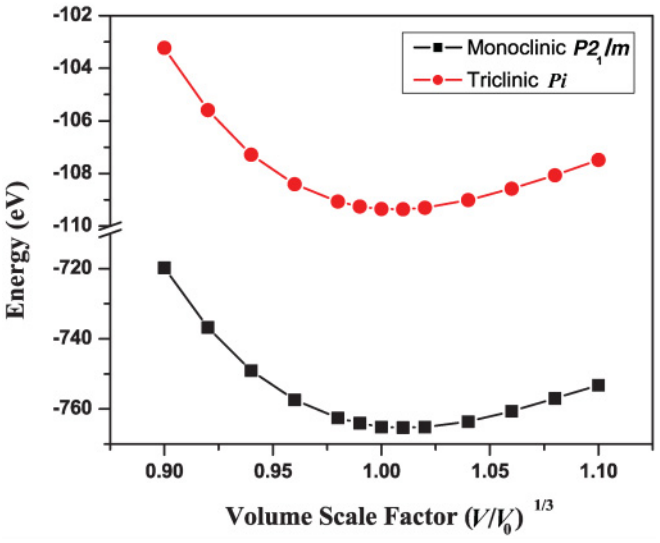

FIG. 2. (Color online) The calculated total binding energy versus cell volume. The volume scale factor is defined as $(V/V_0)^{1/3}$, where V_0 is the experimental equilibrium volume of the unit cell. For monoclinic Li_4SiO_4, $V_0 = 1154.344$ Å^3; for triclinic γ-Li_4SiO_4, $V_0 = 167.214$ Å^3.

Table I compares the experimental measurements with our results. For monoclinic Li_4SiO_4, the predicted structural constants have <1.2% deviation, whereas for triclinic Li_4SiO_4, the deviation is <0.8%. It can also be seen from Table I that the calculated bulk modulus and cohesive energies for these two phases are close to each other.

B. Electronic structural properties

The calculated band structures of these two phases of Li_4SiO_4 are shown in Fig. 3. The bandwidths and gaps are summarized in Table II. The information in Fig. 3 and Table II suggests that the band structures of monoclinic Li_4SiO_4 and triclinic γ-Li_4SiO_4 have some similarities. Both have mainly two VBs, which are located at the energy ranges of $-6.2 \sim 0.0$ eV (VB_1) and $-18.5 \sim -16.0$ eV (VB_2). Within each VB, there are some small gaps. In monoclinic Li_4SiO_4, the width of VB_1 is 2.30 eV, in which a 0.94-eV gap was found and divided the VB_1 into two sub-VBs with widths of 0.42 and 0.94 eV. From Figs. 3(a) and 4(a), it can be seen that the width of its VB_2 is 6.17 eV, which can be divided by a 0.62 eV gap into two sub-VBs with widths of 1.05 and 4.50 eV. The band gap between the VB_1 and the conduction band (CB) of monoclinic Li_4SiO_4 is direct at the Γ high-symmetry point with the value of 5.24 eV. This band gap is much smaller than the value of 17.5 eV that was calculated, based on the LCAO-HF approach, by Munakata and Yokoyama.[15] Usually, the band gap calculated by an HF method is larger than the experimental measurements. However, due to the DFT approximations, which underestimate the excited state energies, our

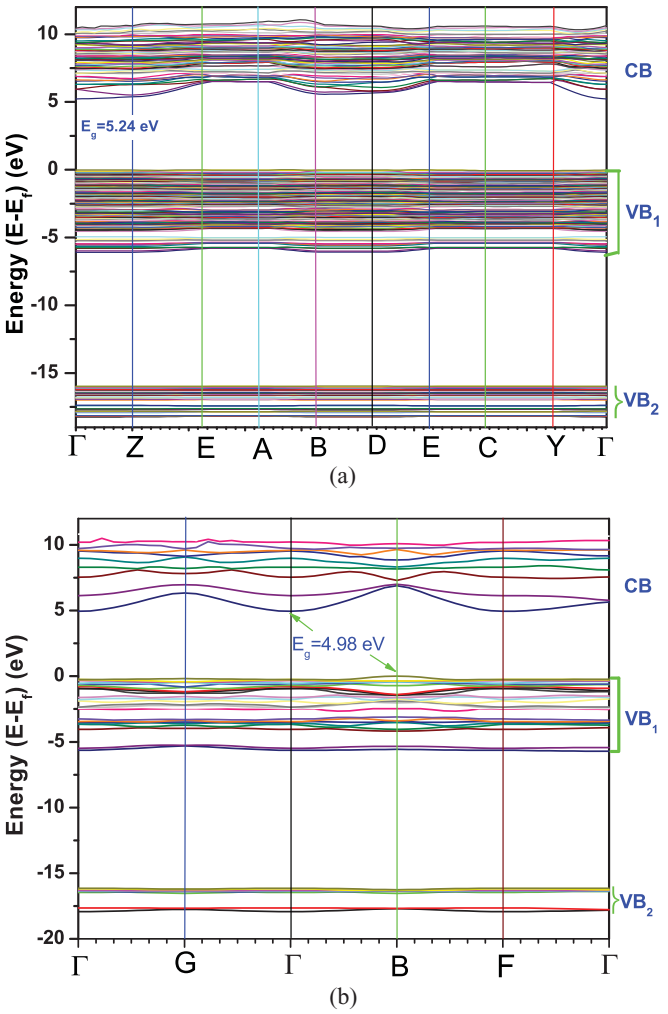

FIG. 3. (Color online) The calculated electronic band structures: (a) monoclinic Li_4SiO_4 and (b) triclinic γ-Li_4SiO_4.

calculated band gap is usually smaller than the experimental measurements.[26] Although there is no experimental band gap available for crystalline Li_4SiO_4, it is expected that the real band gap should be between our DFT predictions and the LCAO-HF values.

The band structure of the triclinic γ-Li_4SiO_4 shown in Fig. 3(b) is similar to that of the monoclinic Li_4SiO_4 shown in Fig. 3(a). The biggest difference is that the calculated band gap in triclinic γ-Li_4SiO_4 is indirect between the **B** and the **Γ** high-symmetry points, as shown in Fig. 3(b), and its value (4.98 eV) is smaller than that of monoclinic Li_4SiO_4. As shown in Table II, the widths of VBs for triclinic γ-Li_4SiO_4 are smaller than those of monoclinic Li_4SiO_4. Similarly, VB_1 of triclinic γ-Li_4SiO_4 is separated by 1.06 eV gap into two sub-VBs with widths of 0.32 and 0.42 eV. Its VB_2 is separated by two gaps (0.85 and 0.32 eV) into three subbands with widths of 0.74, 1.27, and 2.64 eV.

Figure 4 shows the calculated total density of states (TDOS) and partial density of states (PDOS) projected onto Li, O, and Si contributions for both monoclinic and triclinic phases of Li_4SiO_4. In both phases of Li_4SiO_4, the *s* orbital of O mainly contributes to their lower-energy VB_2 and contributes less to their VB_1 and CBs. The *p* orbitals of O contribute to the VB_1 and CBs. The *s* orbital of Si mainly contributes to the lower portions of the VB_1 and VB_2, whereas the *p* orbitals mainly contribute to the higher portions of their VB_1 and VB_2 and both the *s* and *p* orbitals of Si contribute to their CBs. The *s* and *p* orbitals of Li contribute to both phases' VBs and CBs; these *p* orbitals have a higher contribution than the *s* orbital. Interestingly, the portion of VB_1 just below the Fermi level consists mainly of the interactions between the *s* and *p* orbitals of Li and the *p* orbitals of O. However, Munakata and Yokoyama[15] concluded that the contribution of Li is not appreciable to the VBs but is greater in the CBs. Figure 1 shows that in both phases of Li_4SiO_4, the tetrahedral [SiO_4] groups are separated by the surrounding Li coordination. From our results, we found that the tetrahedral [SiO_4] groups in the monoclinic Li_4SiO_4 are partially distorted because only two Si-O bond lengths are equivalent, with an average bond length of 1.68 Å. The other two bonds differ in length, with values of 1.57 and 1.71 Å. Meanwhile, in the triclinic γ-Li_4SiO_4, the tetrahedral [SiO_4] groups are fully distorted, with Si-O bond lengths of 1.348, 1.660, 1.699, and 2.165 Å. And the shortest Li-O bond length in this phase is 1.485 Å, which is much shorter than the Li-O bond lengths in pure Li_2O (1.73 and 1.79 Å).[24]

Based on DFPT,[32–34] the macroscopic static dielectric tensor, including local field effects of the crystal and the Born effective charges tensor for each atom in the unit cell, can be obtained. For both phases, the calculated off-diagonal elements of the macroscopic static dielectric tensor are very small (<0.01), whereas the diagonal elements for monoclinic and triclinic phases of Li_4SiO_4 are 2.687, 2.666, and 2.661 and 2.715, 2.681, and 2.667, respectively. For each atom in the unit cell, the calculated Born effective charges also include the local field effects and can be used to investigate the LO-TO splitting and calculate the IR absorption spectra, as described in the next section. For reference, in Tables S1 and S2 of the supplementary material,[44] we listed the calculated Born effective charge tensors of each nonequivalent atom type and their corresponding optimized coordinates for both monoclinic and triclinic phases of Li_4SiO_4.

C. Phonon dynamical, thermodynamic and optical properties

The calculated phonon dispersions and phonon TDOS of these two phases of Li_4SiO_4 are presented in Figs. 5 and

TABLE II. The calculated band gaps and VB widths of lithium orthosilicates (in electron volts).

Crystal	VB_2 width	Gap between VB_1 and VB_2	VB_1 width	Band gap
Li_4SiO_4	2.30	9.83	6.17	5.24 17.5[a]
γ-Li_4SiO_4	1.80	10.36	5.81	4.98

[a]Ref. 15.

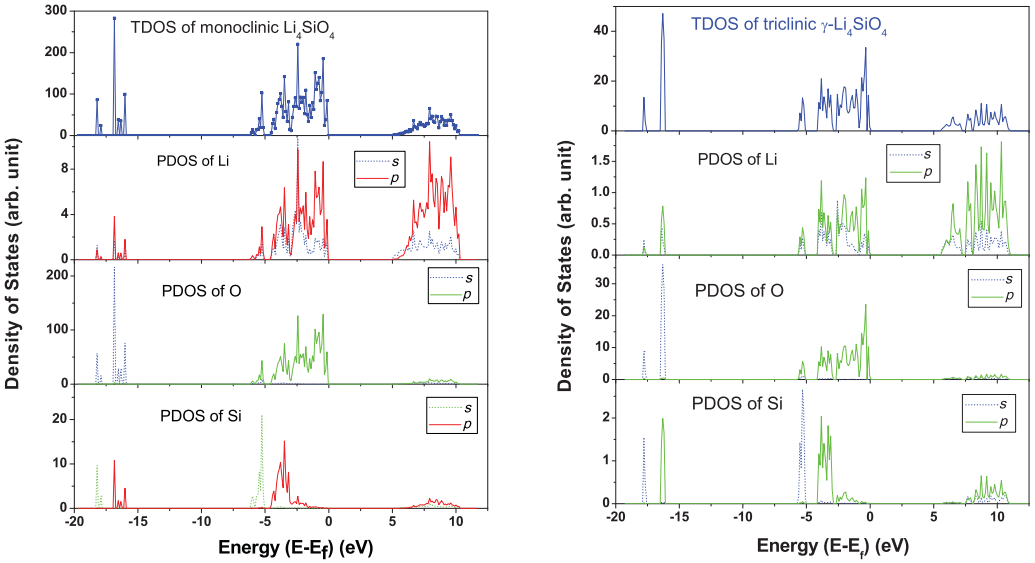

FIG. 4. (Color online) The calculated electronic TDOS and electronic PDOS projected onto each element: (a) monoclinic Li_4SiO_4 and (b) triclinic γ-Li_4SiO_4.

6, respectively. As shown in Table I, the primitive cells of monoclinic Li_4SiO_4 and triclinic γ-Li_4SiO_4 contain 14 and 2 Li_4SiO_4 formula units (f.u.), respectively; therefore, there are 378 branches of phonon modes, as shown in Fig. 5(a), and 54 branches of phonon modes, as shown in Fig. 5(b). Figures 5 and 6 show a frequency gap between 19 and 23 THz for both phases. However, monoclinic Li_4SiO_4 has three soft modes along the wave-vector axis around the **B**, **F**, **Γ**, **Y**, and **A** high-symmetry points, whereas in triclinic γ-Li_4SiO_4, only a single soft mode was found along wave-vector line **Γ**-**S**, where **S** is a point defined later. By taking the average of the calculated macroscopic dielectric constant diagonal elements of crystals and inputting the calculated Born formal charge tensors into the Phonon package,[35] we can see LO-TO splittings at the **Γ** wave-vector in the phonon dispersion curves. From Fig. 5, the triclinic phase of Li_4SiO_4 has a larger LO-TO splitting than the monoclinic phase of Li_4SiO_4, which means that the triclinic phase is more polar and anisotropic than the corresponding monoclinic phase.

By exploring the animations of the soft modes in monoclinic Li_4SiO_4, we found that they are caused by one type of Li, which is shown by the large (green) balls in Fig. 1(a). To confirm that statement, we doubled the displacement of this type of Li atoms to ± 0.06 Å and found that the generated Hellmann-Feynman on-site forces are increased almost exactly by a factor of 2.0. Figure 7 shows the occupation of vibrations of this type of Li in the x, y, and z directions. In these soft modes, the mentioned atoms vibrate mainly in the y and z directions. As discussed in Sec. IIIA, two types of lithium atoms were determined with fully occupancy[40] or half occupancy.[38] In Fig. 1(a), we show the full occupancy with the initial coordinates 4***f***(0.0790, 0.0278, −0.1337) and 2***e***(0.8701, 0.25, 0.2956).[40] After optimization, the positions slightly shifted to 4***f***(0.0830, 0,0225, −0,1300) and 2***e***(−0.1103, 0.25, 0.2817). The symmetry elements of the monoclinic space group generate four Li 4***f***- and two Li 2***e***-equivalent positions.

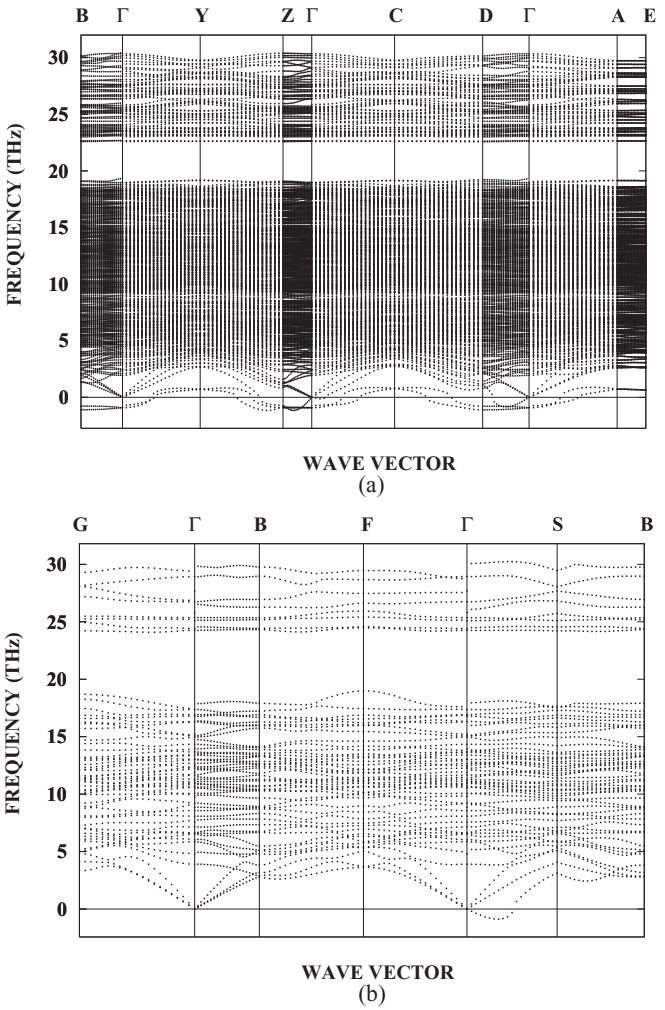

FIG. 5. The calculated phonon dispersion relations with LO-TO splitting: (a) monoclinic Li_4SiO_4 and (b) triclinic γ-Li_4SiO_4.

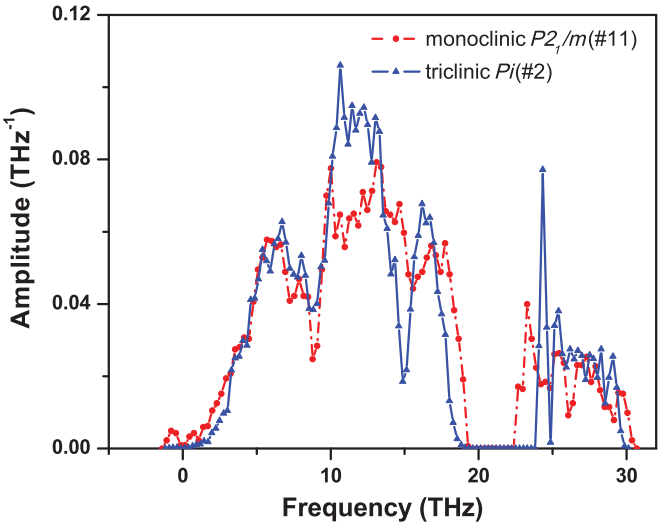

FIG. 6. (Color online) The calculated phonon TDOS for monoclinic Li_4SiO_4 and triclinic γ-Li_4SiO_4.

However, Dejong *et al.*[38] split each of these 4***f*** and 2***e*** positions into two sites (A and B in Table III), leading to eight and four equivalent sites, respectively. These splittings are too close to each other to be occupied by two atoms; therefore, Dejong *et al.*[38] assigned them half Li occupancy. All mentioned pairs with half Li occupancy are given in Table III. Analysis of the polarization vectors of the calculated phonon dispersion curves (Fig. 7) established that the observed soft modes are entirely formed from the vibrations of Li 4***f***, mainly in the y and z directions. Thus, we might expect Li 4***f*** to move in shallow potentials. This state does not lead to a phase transition but rather results in random Li distribution. Polarization vectors of phonon dispersion curves show that 2***e*** lithium do not contribute to soft modes. They vibrate at finite frequencies; hence, we might expect that the minima indicated for Li 2***e*** lithium in Table III are separated by a higher barrier than that of Li 4***f*** and that our optimization process, which uses the confinements of the symmetry elements of the space group, placed Li 2***e*** in one of the double minima potential.

As shown in Fig. 5(b), in triclinic phase the soft mode occurs at an incommensurate wave-vector $q_{\text{in}} = (-0.1869, 0.0930, 0.0759)$ close to $q_c = (-3/16, 1/11, 1/13)$ on the line joining **Γ** point and a general point **S** on the Brillouin zone surface that has a wave-vector equal to $q_{\text{bz}} = (-1/2, 8/33, 8/39)$. The imaginary frequency of this soft mode covers a very small volume of the Brillouin zone. It has an acoustic character with longitudinal vibration of comparable amplitudes for all atoms, because the acoustic phonon dispersion curves depend on the long-range elastic forces. Therefore, we carefully

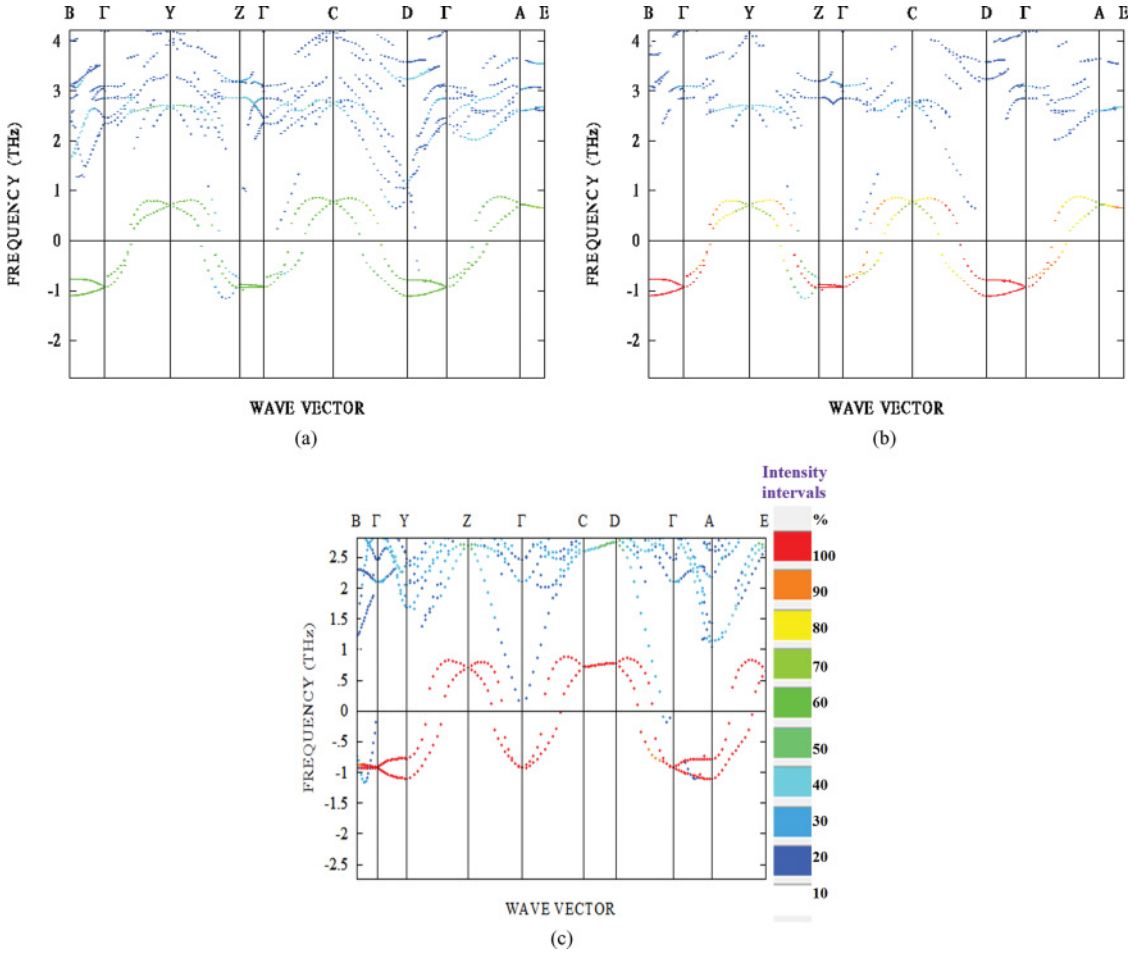

FIG. 7. (Color online) The vibrations of one type of lithium, shown in Fig. 1(a) as large (dark green) balls, in monoclinic Li_4SiO_4: (a) along the x axis, (b) along the y axis, and (c) along the z axis, accompanied by the corresponding color intensity scale.

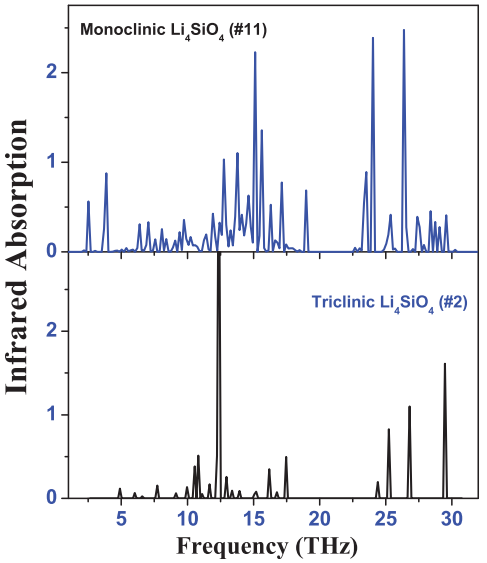

FIG. 8. (Color online) The calculated IR absorption spectra of monoclinic Li_4SiO_4 and triclinic γ-Li_4SiO_4.

treat the found incommensurate soft mode as a proven state, despite even very large supercell (324 atoms) used in this simulation.

Based on the calculated Born effective charge tensor for each nonequivalent atom,[44] the calculated IR absorption spectra for both LO and TO modes of these two phases of Li_4SiO_4 are shown in Fig. 8. It can be seen that monoclinic phase of Li_4SiO_4 has more IR peaks than its corresponding triclinic phase. In the triclinic phase of Li_4SiO_4, with a frequency of $\sim$12.4 THz, there is an absorption peak with highest intensity of 4.7, as shown in the bottom portion of Fig. 8. The optical properties of these two phases of Li_4SiO_4 are different, although their bulk and thermodynamic properties (as discussed in the following paragraphs) have some similarities.

Based on the DFT and phonon dynamics calculations, we can obtain the thermodynamic properties of these two phases of Li_4SiO_4. By ignoring the PV contribution, the free energy of solid Li_4SiO_4 can be obtained by adding the DFT total energy to the phonon free energy. Figure 9 shows the calculated free energy and entropy of the two phases of Li_4SiO_4 versus the temperature. The differences between these two phases are intercalated into the same figure.

Figure 9 also shows that the differences between these two phases are small—within 2 kJ/mol in free energy and 5 J/mol K in entropy. As shown in Fig. 9(a), throughout the temperature range, the free energy of the monoclinic phase of Li_4SiO_4 is higher than that of the triclinic phase of Li_4SiO_4, although the difference is quite small (within 2 kJ/mol). These results indicate that the triclinic phase is slightly more stable than the monoclinic phase of Li_4SiO_4. Actually, the experimental synthesis of triclinic Li_4SiO_4 is at a low temperature and without disorder,[41] whereas the monoclinic Li_4SiO_4 could include disordered lithium atoms.[38,40] From the thermodynamic point of view, our results showed that there is no big energetic difference between these two phases of Li_4SiO_4.

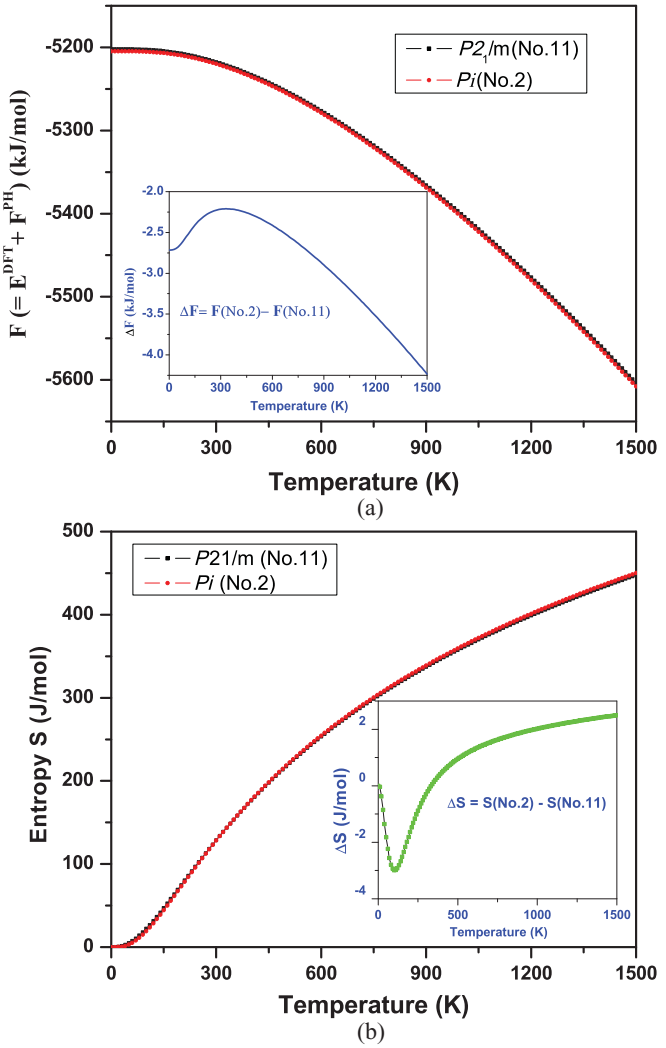

FIG. 9. (Color online) The calculated thermodynamic properties. (a) The total free energies and the differences between these two phases. The total free energy for each phase is the sum of phonon free energy and the corresponding DFT energy, which are -5273.77 kJ/mol for monoclinic Li_4SiO_4 and -5275.56 kJ/mol for triclinic γ-Li_4SiO_4. (b) The entropies and the corresponding differences between these two phases.

D. Capabilities of CO_2 capture

From experimental investigations, Li_4SiO_4 and Li_2ZrO_3 are good candidates of solid sorbents for CO_2 capture in terms of large CO_2 sorption capacity, infinite CO_2/N_2 or CO_2/H_2 selectivity, good reversibility, and high operating temperature,[13,14,24,25,45–51] based on the following reactions:

(1) $Li_4SiO_4 + CO_2 = Li_2CO_3 + Li_2SiO_3$

(2) $Li_2ZrO_3 + CO_2 = Li_2CO_3 + ZrO_2$

By assuming that the difference between the chemical potentials ($\Delta\mu^\circ$) of the solid phases of Li_2SiO_3 and Li_4SiO_4 and gas CO_2 molecule can be approximated by the difference in their total energies (ΔE^{DFT}), obtained directly from DFT calculations, and the vibrational free energy of the phonons (ΔF^{PH}, excluding zero-point energy, which was already counted into the term ΔE_{ZP}) and by ignoring the PV contribution terms for solids, as described in our previous

papers,[24,25,28] the variation of the chemical potential ($\Delta\mu$) for reaction 1 with temperature and pressure can be written as

$$\Delta\mu(T,P) = \Delta\mu^0(T) - RT \ln P_{CO_2}, \quad (2)$$

where

$$\Delta\mu^0(T) \approx \Delta E^{DFT} + \Delta E_{ZP} + \Delta F^{PH}(T) - G_{CO_2}(T). \quad (3)$$

In addition, the heat of reaction, or $\Delta H^{cal}(T)$, for reaction 1 can be evaluated through the equation

$$\Delta H^{cal}(T) = \Delta\mu^0(T) + T[\Delta S^{PH}(T) - S_{CO_2}(T)], \quad (4)$$

where $\Delta S^{PH}(T)$ is the entropy difference between Li_2SiO_3 and Li_4SiO_4 and where $G_{CO2}(T)$ and $S_{CO2}(T)$ are the Gibbs free energy and entropy of gas CO_2 that can be obtained from the standard statistical mechanics[52] and the thermodynamic database, respectively.[53]

Based on Eq. (4), the calculated heat of reactions (enthalpy change) for these reactions with both monoclinic and triclinic phases of Li_4SiO_4 versus the temperatures are plotted in Fig. 10(a). For comparison, the available experimental data for the reaction of $2Li_2O^*SiO_2$ capturing CO_2 from the HSC Chemistry database[54] and Li_2ZrO_3 capturing CO_2 data taken from Ref. 27 were also plotted in Fig. 10(a). The calculated heat of reactions for both phases of Li_4SiO_4 are quite close to each other, with a <3 kJ/mol difference. At a low temperature ($T < 400$ K), the calculated heat of reaction is very close to the value obtained from the HSC Chemistry database.[54] However, with the increase in temperature, the discrepancy between the calculated and the HSC data becomes larger. There are two main reasons for such a large discrepancy at higher temperatures. First, because our calculations are based on the assumption that except for CO_2 all materials are perfect crystalline solids and their low-temperature structures were used to represent the structures over the entire temperature range, as discussed in our previous work,[28] a larger discrepancy is possible and indicates that some caution should be exercised in the use of these data at a high temperature. It is well known that the binding energy of a gas molecule reacting with a solid exhibits large errors when a local density approximation or generalized gradient approximation is used.[55] This means that a large discrepancy in enthalpy change for reactions involving gas–solid phases is possible because the self-interaction is not canceled when forming new compounds. Another reason for such a large discrepancy concerns the experimental related measurement. Experimentally, Li_4SiO_4 and Li_2SiO_3 were synthesized by mixing Li_2CO_3 and SiO_2 with 2:1 and 1:1 molar ratio and were heat treated at a high temperature.[47,56] Therefore, the experimental samples may not be exactly the perfect crystalline Li_4SiO_4 and Li_2SiO_3. Instead, they may exist in the mixed forms, such as $2Li_2O^*SiO_2$ and $Li_2O^*SiO_2$, as denoted in the HSC Chemistry database.[54] Such a mismatched structure of the material can create some discrepancies. Compared to Li_4SiO_4, Fig. 10(a) shows that the reaction heat of Li_2ZrO_3 capturing CO_2 is ~20 kJ/mol lower, indicating that more heat is needed for regenerating Li_2ZrO_3 back from Li_2CO_3 and ZrO_2.

Based on Eq. (2), the dependence of the chemical potential $\Delta\mu(T,P)$ on temperature and the CO_2 pressure P_{CO2} is shown in Fig. 10(b). The line in Fig. 10(b) indicates that for each reaction, $\Delta\mu(T,P)$ is approaching zero. The region close to the line is favorable for absorption and desorption because of the minimal energy costs at a given temperature and pressure. Above the line, the solid (Li_4SiO_4 and Li_2ZrO_3) is favorable to absorb CO_2 and form Li_2CO_3, whereas below the line, Li_2CO_3 is favorable to release CO_2 and regenerate lithium silicate solids. Although Li_2SiO_3 could absorb CO_2 to further reduce to SiO_2 and Li_2CO_3, experimental results showed that the kinetic behavior of CO_2 absorption on Li_2SiO_3 is much slower than that on Li_4SiO_4.[14,50] Therefore, upon capturing CO_2, Li_4SiO_4 only forms Li_2SiO_3; it does not further decompose to SiO_2.

As described previously and shown in Fig. 10(b), the reaction of Li_4SiO_4 capturing CO_2 is thermodynamically favorable over quite a range of temperatures (<900 K) and P_{CO2}, which means that under this temperature range CO_2 is thermodynamically favored by Li_4SiO_4. But as a CO_2 solid sorbent, the sorbent not only easily absorb the CO_2 in the first half cycle but also easily release the CO_2 from products (e.g., Li_2CO_3 and Li_2SiO_3) in the second half cycle. The operating conditions for the absorption/desorption processes depend on the pre- and postcombustion technologies. Under precombustion conditions, after water–gas shifting, the gas stream mainly contains CO_2, H_2O, and H_2. The partial CO_2 pressure is ~20–25 bar, and the temperature is ~573–623 K. To minimize energy consumption, the ideal sorbents should work at these pressure and temperature ranges to separate CO_2 from H_2. From Fig. 10(b), the corresponding temperatures for monoclinic Li_4SiO_4 and triclinic Li_4SiO_4 are 1030 K and 1010 K, respectively, which are higher than the precombustion

TABLE III. The double site atomic positions in the monoclinic structure, with an average half occupancy of lithium atoms as suggested by Dejong *et al.* (Ref. 38). The last two rows contain nonequivalent lithium positions obtained after present *ab initio* optimization. Position 4***f*** is between the **A** and the **B** minima, whereas position 2***e*** is beyond both the **A** and the **B** minima.

Atom	Minimum **A**	Minimum **B**
1. 4***f***	0.0887, 0.0460, −0.1241	0.0522, −0.0436, −0.1553
2. 4***f***	0.9113, 0.5460, 0.1241	0.9478, 0.4564, 0.1553
3. 4***f***	0.9113, −0.0460, 0.1241	0.9478, 0.0436, 0.1553
4. 4***f***	0.0887, 0.4540, −0.1241	0.0522, 0.5436, −0.1557
5. 2***e***	−0.1444, $\frac{1}{4}$, 0.2978	−0.1191, $\frac{1}{4}$, 0.2875
6. 2***e***	0.1444, $\frac{3}{4}$, 0,7022	0.1191, $\frac{3}{4}$, 0.7125
1. 4***f***	0.0830, 0.0225, −0.1300	Values obtained after *ab initio* optimization based on Tranqui *et al.* (Ref. 40) measurements
5. 2***e***	−0.1103, $\frac{1}{4}$, 0.2817	

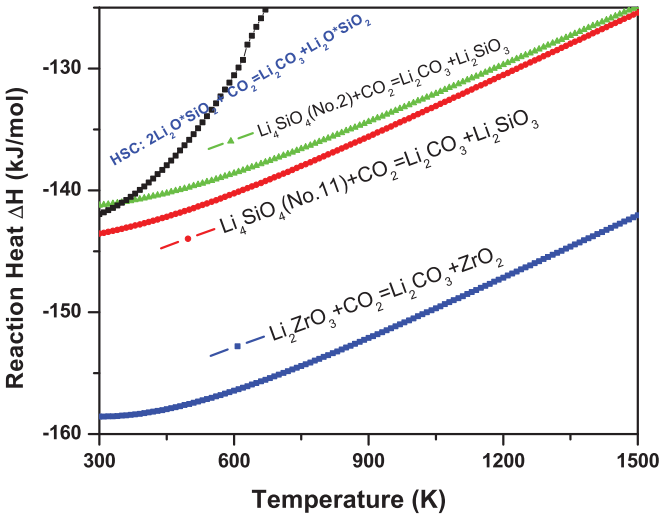

(a)

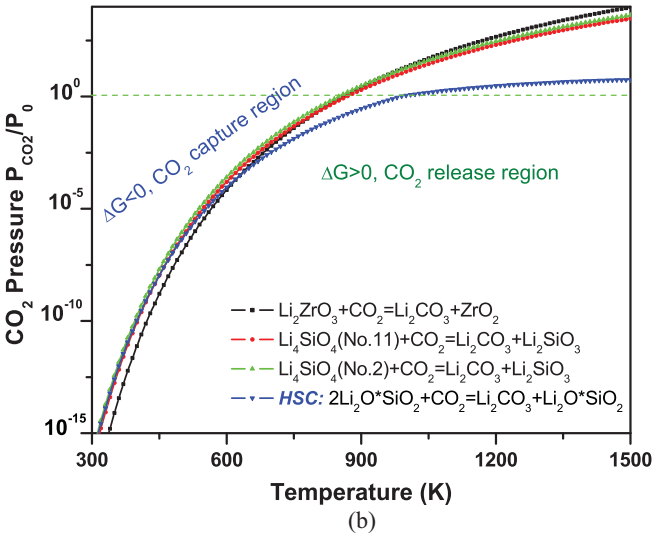

(b)

FIG. 10. (Color online) The calculated thermodynamic properties of the reactions of lithium silicate capturing CO_2. For comparison, the data of lithium zirconate (Ref. 27) are also plotted in the figure. The data of $Li_2O^*SiO_2$ and $2Li_2O^*SiO_2$ from the HSC Chemistry database (Ref. 54) are also presented in the figure. (a) The heat of reaction versus temperature. (b) The contour plotting of calculated chemical potential ($\Delta\mu$) versus temperature and the CO_2 pressure (P plotted in the logarithmic scale) for the CO_2 capture reactions. Only the $\Delta\mu = 0$ curve is shown explicitly. For each reaction, above the $\Delta\mu = 0$ curve $\Delta\mu < 0$, which means the sorbents absorb CO_2 and the reaction goes forward, whereas below the $\Delta\mu = 0$ curve $\Delta\mu > 0$, which means the CO_2 starts to release and the reaction goes backward to regenerate the sorbents.

temperature (573∼623K) conditions. For postcombustion conditions, the gas stream mainly contains CO_2 and N_2, the partial pressure of CO_2 is ∼0.1–0.2 bar, and the temperature range is quite different. The US Department of Energy programmatic goal for postcombustion CO_2 capture technology is to capture at least 90% CO_2 with a cost in electricity of no more than 35%, whereas the goal precombustion CO_2 capture is to capture at least 90% CO_2 with a cost in electricity of no more than 10%.[57,58] From Fig. 10(b), the turnover temperatures for postcombustion capture by these two phases of Li_4SiO_4 are 780 K and 770 K, respectively, which is ∼100 K less than the experimental data.[13,47] As we discussed previously, this discrepancy could be caused by the mismatched crystal structures of solids at higher temperatures.

Based on reactions 1 and 2, the theoretical capacity of Li_4SiO_4 for CO_2 capture is 36.71 weight percent (wt%), and for Li_2ZrO_3 it is 28.74 wt%. From Fig. 10(a), the regenerating heat for Li_2ZrO_3 is higher than that of Li_4SiO_4. Li_4SiO_4 can be synthesized by Li_2CO_3 and SiO_2, and Li_2ZrO_3 can be synthesized by Li_2CO_3 and ZrO_2. Li_4SiO_4 is lighter and much cheaper than Li_2ZrO_3. Therefore, as a high-temperature CO_2 sorbent, Li_4SiO_4 is better suited than Li_2ZrO_3. These conclusions are in good agreement with experimental results, in which the weight change due to CO_2 capture for Li_4SiO_4 is ∼50% greater than that of Li_2ZrO_3[13,47] and the experimental maximum CO_2 absorption capacity has reached 36.66 wt%,[14] which is very close to the theoretical maximum capacity (36.71 wt%).

IV. CONCLUSIONS

In this study, the bulk, electronic, lattice dynamical, optical, thermodynamic, and CO_2 capture properties of monoclinic and triclinic phases of Li_4SiO_4 have been investigated by combining DFPT with phonon lattice dynamics calculations. We found some similarities between these two phases. The calculated bulk modulus and the cohesive energies of these two phases are close to each other.

The band structures of both monoclinic and triclinic phases of Li_4SiO_4 have mainly two VBs. Their VB_1 are located just below the Fermi level and have widths of 6.17 and 5.81 eV, respectively, and their VB_2 are located below −16 eV and have narrow bandwidths of 2.30 and 1.80 eV, respectively. Interestingly, the monoclinic phase of Li_4SiO_4 has a direct band gap of 5.24 eV, whereas the triclinic Li_4SiO_4 phase has an indirect band gap of 4.98 eV. In both phases of Li_4SiO_4, the s orbital of O mainly contributes to the lower-energy VB_2 and the p orbitals contribute to the VB_1 and CBs. The s orbital of Si mainly contributes to the lower portions of the VB_1 and VB_2, and the p orbitals mainly contribute to the higher portions of their VB_1 and VB_2. The s and p orbitals of Li contribute to both phases' VBs and CBs, and these p orbitals have a higher contribution than the s orbital.

The phonon dispersions and phonon densities of states for both phases of Li_4SiO_4 were calculated by the direct method. In triclinic γ-Li_4SiO_4, a possible soft mode was found; in the monoclinic Li_4SiO_4, there are three soft modes that correspond to the one type of Li, which remains disordered over more lattice sites. The LO-TO splitting in triclinic phase of Li_4SiO_4 is larger than that of monoclinic phase of Li_4SiO_4, which indicates the triclinic phase is more polar and anisotropic than the corresponding monoclinic phase.

Based on the calculated IR absorption spectra for both LO and TO modes of these two phases of Li_4SiO_4 and their band structures, it can be concluded that the optical properties of these two phases of Li_4SiO_4 are different, although their bulk and thermodynamic properties remain quite similar.

At a low temperature (<500 K), the calculated heat of reaction of $Li_4SiO_4 + CO_2 \leftrightarrow Li_2CO_3 + Li_2SiO_3$ is in good agreement with the experimental data. From the calculated relationship of the chemical potential of the capture reaction

versus temperatures and CO_2 pressures, Li_4SiO_4 could be a good candidate as high-temperature CO_2 sorbent used for postcombustion capture technology. Compared to Li_2ZrO_3, Li_4SiO_4 is the better choice because of cheaper material cost and higher CO_2 capacity.

ACKNOWLEDGMENTS

Y.D. expresses his gratitude to D. C. Sorescu, H. P. Loh, and R. Anderson for fruitful discussions and for reading the manuscript.

*yuhua.duan@netl.doe.gov

[1] M. A. K. L. Dissanayake and A. R. West, J. Mater. Chem. **1**, 1023 (1991).
[2] R. Collongues, A. Kahn, and D. Michel, Annu. Rev. Mater. Sci. **9**, 123 (1979).
[3] K. Okuno and H. Kudo, Fusion Eng. Des. **8**, 355 (1989).
[4] K. Moritani, T. Magari, and H. Moriyama, Fusion Eng. Des. **39–40**, 675 (1998).
[5] K. Munakata, A. Baba, T. Kawagoe, T. Takeishi, Y. Yokoyama, M. Nishikawa, R. D. Oenzhorn, and K. Okuno, J. Nucl. Sci. Tech. **36**, 962 (1999).
[6] D. Cruz, S. Bulbulian, E. Lima, and H. Pfeiffer, J. Solid State Chem. **179**, 909 (2006).
[7] S. Claus, H. Kleykamp, and W. Smykatz-Kloss, J. Nucl. Mater. **230**, 8 (1996).
[8] H. Pfeiffer and K. M. Knowles, J. Eur. Ceram. Soc. **24**, 2433 (2004).
[9] K. Nakagawa and T. Ohashi, J. Electrochem. Soc. **145**, 1344 (1998).
[10] K. Nakagawa and T. Ohashi, Electrochemistry **67**, 618 (1999).
[11] M. Olivares-Marin, T. C. Drage, and M. M. Maroto-Valer, Int. J. Greenh. Gas Con. **4**, 623 (2010).
[12] M. Kato and K. Nakagawa, J. Ceram. Soc. Jpn. **109**, 911 (2001).
[13] K. Essaki, K. Nakagawa, M. Kato, and H. Uemoto, J. Chem. Eng. Jpn. **37**, 772 (2004).
[14] R. Rodriguez-Mosqueda and H. Pfeiffer, J. Phys. Chem. A **114**, 4535 (2010).
[15] K. Munakata and Y. Yokoyama, J. Nucl. Sci. Tech. **38**, 915 (2001).
[16] T. Uchino and T. Yoko, J. Phys. Chem. B **103**, 1854 (1999).
[17] T. Uchino and T. Yoko, J. Phys. Chem. B **102**, 8372 (1998).
[18] W. Y. Ching, Y. P. Li, B. W. Veal, and D. J. Lam, Phys. Rev. B **32**, 1203 (1985).
[19] J. C. Du and L. R. Corrales, J. Non-Cryst. Solid. **352**, 3255 (2006).
[20] J. C. Du and L. R. Corrales, J. Phys. Chem. B **110**, 22346 (2006).
[21] T. Nakazawa, K. Yokoyama, V. Grismanovs, and Y. Katano, J. Nucl. Mater. **279**, 201 (2000).
[22] G. Kresse and J. Hafner, Phys. Rev. B **47**, 558 (1993).
[23] G. Kresse and J. Furthmuller, Comp. Mater. Sci. **6**, 15 (1996).
[24] Y. Duan and D. C. Sorescu, Phys. Rev. B **79**, 014301 (2009).
[25] Y. Duan and D. C. Sorescu, J. Chem. Phys. **133**, 074508 (2010).
[26] Y. Duan, Phys. Rev. B **77**, 045332 (2008).
[27] Y. Duan, J. Renew. Sust. Energ. **3**, 013102 (2011).
[28] Y. Duan, B. Zhang, D. C. Sorescu, and J. K. Johnson, J. Solid State Chem. **184**, 304 (2011).
[29] J. P. Perdew and Y. Wang, Phys. Rev. B **45**, 13244 (1992).
[30] H. J. Monkhorst and J. D. Pack, Phys. Rev. B **13**, 5188 (1976).
[31] C. J. Bradley and A. P. Cracknell, *The Mathematical Theory of Symmetry in Solids* (Clarendon Press, Oxford, 1972).
[32] S. Baroni, P. Giannozzi, and A. Testa, Phys. Rev. Lett. **58**, 1861 (1987).
[33] M. Gajdos, K. Hummer, G. Kresse, J. Furthmuller, and F. Bechstedt, Phys. Rev. B **73**, 045112 (2006).
[34] X. Gonze, Phys. Rev. A **52**, 1086 (1995).
[35] K. Parlinski, Phonon software package (2010).
[36] X. Gonze and C. Lee, Phys. Rev. B **55**, 10355 (1997).
[37] K. Parlinski, Z. Q. Li, and Y. Kawazoe, Phys. Rev. Lett. **78**, 4063 (1997).
[38] B. H. W. S. Dejong, D. Ellerbroek, and A. L. Spek, Acta Crystallogr. B **50**, 511 (1994).
[39] H. Vollenkl, A. Wittmann, and H. Nowotny, Monatsh. Chem. **99**, 1360 (1968).
[40] D. Tranqui, R. D. Shannon, H. Y. Chen, S. Iijima, and W. H. Baur, Acta Crystallogr. B **35**, 2479 (1979).
[41] R. Hoppe, K. Bernet, and A. Moller, Z. Anorg. Allg. Chem. **629**, 1285 (2003).
[42] F. D. Murnaghan, Am. J. Math. **59**, 235 (1937).
[43] F. Birch, Phys. Rev. **71**, 809 (1947).
[44] See Supplemental Material at http://link.aps.org/supplemental/10.1103/PhysRevB.84.104113 for Born effective charge tensors.
[45] K. Essaki, M. Kato, and K. Nakagawa, J. Ceram. Soc. Jpn. **114**, 739 (2006).
[46] K. Essaki, M. Kato, and H. Uemoto, J. Mater. Sci. **40**, 5017 (2005).
[47] M. Kato, S. Yoshikawa, and K. Nakagawa, J. Mater. Sci. Lett. **21**, 485 (2002).
[48] T. Okumura, K. Enomoto, N. Togashi, and K. Oh-Ishi, J. Ceram. Soc. Jpn. **115**, 491 (2007).
[49] T. Okumura, Y. Matsukura, K. Gotou, and K. Oh-Ishi, J. Ceram. Soc. Jpn. **116**, 1283 (2008).
[50] M. J. Venegas, E. Fregaso-Israel, R. Escamilla, and H. Pfeiffer, Ind. Eng. Chem. Res. **46**, 2407 (2007).
[51] T. Yamaguchi, T. Niitsuma, B. N. Nair, and K. Nakagawa, J. Membr. Sci. **294**, 16 (2007).
[52] R. G. Mortimer, *Physical Chemistry* (Academic Press, London, 2000).
[53] D. R. Lide, *Handbook of Chemistry and Physics* (CRC Press, Boca Raton, Florida, 2002).
[54] "HSC Chemistry Software 6.1" [http://www.outotec.com/hsc] (Outotec Research, Pori, Finland, 2006).
[55] L. Wang, M. Maxisch, and G. Ceder, Phys. Rev. B **73**, 195107 (2006).
[56] H. Migge, J. Nucl. Mater. **151**, 101 (1988).
[57] DOE-NETL: "Cost and Performance Baseline for Fossil Energy Plants," Vol. 1: *Bituminous Coal and Natural Gas to Electricity Final Report* [http://www.netl.doe.gov/energy-analyses/baseline_studies.html] (Nov. 2010).
[58] J. D. Figueroa, T. Fout, S. Plasynski, H. McIlvried, and R. D. Srivastava, Int. J. Greenh. Gas Con. **2**, 9 (2008).